frontiers | Frontiers in Earth Science

TYPE Original Research
PUBLISHED 09 September 2022
DOI 10.3389/feart.2022.1012607

OPEN ACCESS

EDITED BY
Hu Li,
Southwest Petroleum University, China

REVIEWED BY
Qin Zhang,
China University of Petroleum, Beijing, China
Qrong Qin,
Southwest Petroleum University, China

*CORRESPONDENCE
Chao Gao,
ycgaochao@qq.com

SPECIALTY SECTION
This article was submitted to Structural Geology and Tectonics, a section of the journal Frontiers in Earth Science

RECEIVED 05 August 2022
ACCEPTED 18 August 2022
PUBLISHED 09 September 2022

CITATION
Wang X, Liang Q, Gao C, Xue P, Yin J and Hao S (2022), Hydrocarbon accumulation model influenced by "three elements (source-storage-preservation)" in lacustrine shale reservoir-A case study of Chang 7 shale in Yan'an area, Ordos Basin. *Front. Earth Sci.* 10:1012607. doi: 10.3389/feart.2022.1012607

Hydrocarbon accumulation model influenced by "three elements (source-storage-preservation)" in lacustrine shale reservoir-A case study of Chang 7 shale in Yan'an area, Ordos Basin

Xiangzeng Wang, Quansheng Liang, Chao Gao*, Pei Xue, Jintao Yin and Shiyan Hao

Shaanxi Yanchang Petroleum (Group) Corp., Ltd., Xi'an, China

The organic-rich shales of the Chang 7 Member in the Yan'an Formation of the Yan'an area, Ordos Basin is a hot spot for lacustrine shale gas exploration. In this paper, taking the Chang 7 Member shale in the Yan'an area as an example, the main controlling factors of lacustrine shale gas accumulation and the prediction of "sweet spots" are systematically carried out. The results show that the Yanchang Formation shale has the complete gas generating conditions. Shale gas accumulation requires three necessary accumulation elements, namely gas source, reservoir and good preservation conditions. The dynamic hydrocarbon generation process of the Chang 7 shale reservoirs is established according to the thermal simulation experiments of hydrocarbon generation, and the mechanism of catalytic degradation and gas generation in the Chang 7 Member under the background of low thermal evolution degree is revealed. The enriched authigenic pyrite can catalyze the hydrocarbon generation of organic matter with low activation energy, thereby increasing the hydrocarbon generation rates in the low-mature-mature stage. Different types of pores at different scales (2–100 nm) form a multi-scale complex pore network. Free gas and dissolved gas are enriched in laminar micro-scale pores, and adsorbed gas is enriched in nano-scale pores of thick shales, and silty laminates can improve the physical properties of the reservoir. This is because the laminar structure has better hydrocarbon generation conditions and is favorable for the migration of oil and gas molecules. The thickness of the lacustrine shale in the Chang 7 Member is between 40 and 120 m, which has exceeded the effective hydrocarbon expulsion thickness limit (8–12 m). At the end of the Early Cretaceous, the excess pressure of the Chang 7 shale was above 3 MPa. At present, horizontal wells with a daily gas production of more than 50,000 cubic meters are distributed in areas with high excess pressures during the maximum burial depth.

KEYWORDS

Ordos Basin, lacustrine shale gas, hydrocarbon generation, storage, accumulation model

1 Introduction

Organic-rich shale is widely developed in China, and the shale gas resource potential is huge (Ji et al., 2012; Zhao et al., 2016; Fan et al., 2020; Zheng et al., 2020). According to the sedimentary geological conditions, it is divided into marine shale, continental shale and marine-continental transitional shale (Lama and Vutukuri, 1978; Wu and Yu, 2007; Yang et al., 2016; Hong et al., 2020; Mahmud et al., 2020; Katz et al., 2021; Lan et al., 2021; Qie et al., 2021). Under the guidance of the theory of "binary control of hydrocarbon enrichment" of highly evolved marine shale gas in complex structural areas, the first large-scale shale gas field, i.e., Fuling Gas Field, was discovered in the southern China on 28 November 2012. Two-thirds of China's shale gas resources are distributed in lacustrine shale sedimentary strata. The current research practice has confirmed that the maturity of lacustrine shales in China is low (oil generation stage), and the gas generating range is small. How to find large-scale hydrocarbon accumulation areas is the main challenge of shale oil and gas exploration in China (Sun et al., 2017; Xu et al., 2019; Xue et al., 2021).

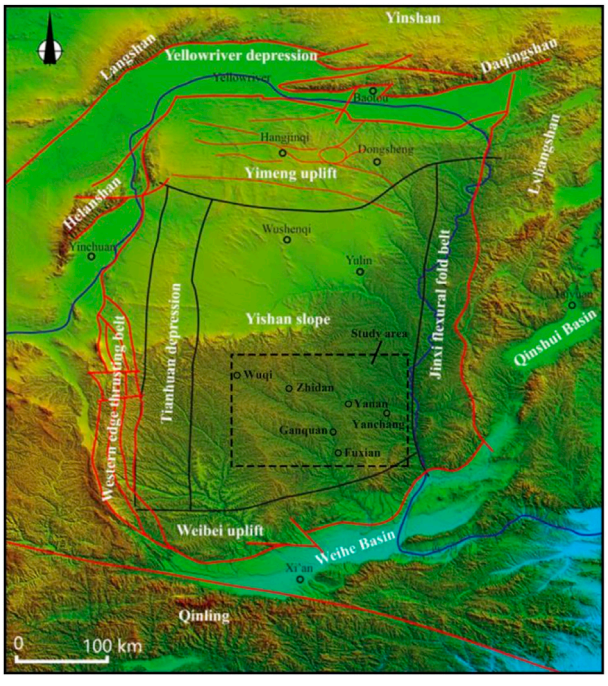

FIGURE 1
Location of the study area (modified by Xu et al., 2022).

The geological resources of lacustrine shale gas in the Ordos Basin are 2.42 × 10^{12} m^3. With the gradual breakthrough of lacustrine shale gas production and the continuous deepening of research work, the exploration of shale gas enrichment areas and high-yield areas has become the focus of current hydrocarbon exploration. Compared with marine shale, the reservoir heterogeneity of lacustrine shale is stronger (Ursula and Jorge., 2014; Liang et al., 2016; Li et al., 2019; Yu K. et al., 2019; Asante-Okyere et al., 2021). In addition, lacustrine shale also has the characteristics of high clay mineral content, high adsorbed gas ratio, low thermal evolution degree, low brittle mineral content, and low formation pressure. Therefore, the accumulation law of lacustrine shale gas is more complex, and its requirements for the oil and gas development technology are higher (Sun et al., 2017; Xu et al., 2019; Santosh and Feng., 2020; Vafaie et al., 2021). The mechanism of lacustrine shale gas accumulation has become a hot issue that has attracted much attention. In this paper, taking the Chang 7 Member shale in the Yan'an area as an example, the main controlling factors of lacustrine shale gas accumulation and the prediction of "sweet spots" are systematically carried out based on a large number of geochemical and reservoir characterization experiments. This study can provide a theoretical basis for supporting further exploration and development of lacustrine shale gas.

2 Databases and methods

2.1 Geological background

The study area is located in the southeastern part of the Ordos Basin, and the administrative area belongs to the Yan'an City, Shaanxi Province (Figure 1). Low-amplitude uplifts in the Ordos Basin are well developed. This area presents a regional slope that tilts from the east to the west. Several sets of organic-rich shale are deposited in the study area. The burial depth of the Chang 7 Member of the Mesozoic Yanchang Formation is between 500 and 2,000 m, which has good geological conditions and resource base for shale gas accumulation.

The sedimentary period of the Chang 7 Member was the heyday of the development of the lake basin, and it belonged to the sedimentary environment of shallow lacustrine to semi-deep lacustrine facies. 50–80 m shales ("Zhangjiatan" shale) are developed in the Chang 7 Member in the study area. The average clay mineral content of the Chang 7 shale is 46.71%, and the average content of the quartz and feldspar is 27.77% and 16.83%, respectively. In fact, the Chang 7 Member shale has lower brittle mineral content and stronger plasticity.

TABLE 1 Geochemical parameters of the Chang 7 Member samples of the hydrocarbon generation kinetic pyrolysis experiments.

Well	Depth (m)	Lithology	TOC (%)	S1 (mg/g)	S2 (mg/g)	S3 (mg/g)	TMAX (°C)	IH (mg/g·TOC)	IO (mg/g·TOC)
DT005	687.9	Shale	2.23	1.22	6.53	0.22	443	292	9

2.2 Materials and methods

2.2.1 Thermal simulation experiments of hydrocarbon generation

In this study, the Chang 7 shale samples from the Well DT005 in the study area were selected for the hydrocarbon generation kinetic experiments. The geochemical characteristics of the samples are listed in Table 1. It can be seen from Table 1 that the burial depth of the samples is 687.9 m. The TOC of the samples was 2.23%, the hydrogen index was 292 mg/g·TOC, and the T_{max} was 443°C. This shows that the thermal evolution degree of the samples is relatively low, which meets the requirements of the hydrocarbon generation kinetic pyrolysis experiments. In this experiment, an open system hydrocarbon generation kinetics pyrolysis experiment was used, and the open system hydrocarbon generation kinetics experiment could exclude secondary cracking during the experiments.

2.2.2 Experiments on pore structures and fluid occurrence

The instrument for analyzing the physical properties of tight rocks such as shale is the SPEC-PMR-20M nuclear magnetic resonance core analyzer. The main technical parameters and functions of the instrument are as follows: magnetic field frequency: 20 M; test area: Φ 25 mm × 40 mm cylinder. First, the pore structures and porosity of the organic matter in the sample before extraction are tested, which is the pore volume occupied by free gas (assuming that it is fully occupied by shale gas), that is, the gas-bearing porosity. The gas porosity minus the pore volume of adsorbed gas is the pore volume occupied by free gas. Then, an organic solvent was used to extract the chloroform pitch "A" content of the samples. The obtained porosity is the sum of the volume of liquid oil and gas-containing pores, namely the hydrocarbon-containing porosity; the difference between the porosity and the gas-containing porosity is the oil-containing porosity. Dissolved gas can be calculated according to the solubility of shale gas in liquid hydrocarbons and the saturations of oil.

3 Results

3.1 Development characteristics of high-quality source rocks

The TOC content of the Chang 7 shale in the study area is mainly distributed between 3% and 6%, with an average of 4.8%. However, it can be seen from the analysis of pyrolysis parameters and the triangular map of micro-composition (Figure 2A) that the sum of the exinite and inertic components of the Chang 7 shale basically exceeds 55%. It shows that the hydrogen-rich components favorable for hydrocarbon generation are abundant, which lays a material foundation for the generation of shale gas. The organic matter type of the Chang 7 Member is mainly Type II_1, followed by Type II_2, and there is no Type I organic matter. Its R_o is mainly distributed in 0.7%–1.2%. It belongs to high-quality source rock and is the main source rock of the Yanchang Formation.

From the chemical structures of microcomponents and their hydrocarbon-generating properties, it can be seen that the vitrinite is richer in short-chain alkyl groups than saprolite and chitinite, which is beneficial to the generation of natural gas. Therefore, the higher gas generation rate of the Yanchang Formation shale in the low-mature-mature evolution stage is closely related to the mixed organic matter composition of terrigenous higher plants and lower organisms (Figure 2B). The organic matter composition of the Barnett low-mature shales contain more than 80% asphaltene bodies (exinite), and the content of vitrinite is very low, which is obviously different from the Yanchang Formation shales. The gas generation activation energy of the Chang 7 shale is lower than that of the Barnett shale, which is favorable for a large amount of gas generation in the early stage of thermal evolution of the Chang 7 shale. The TOC of the Barnett shale sample used in the experiment is 5.51%, the R_o is 4.4%, and the organic matter type is Type II. Compared with the experimental samples in this study, the Barnett shale samples are less mature and the experimental heating rate is slightly lower. Comparative analysis shows that the average activation energy of kerogen gas generation in the Yanchang Formation shale is 56 kcal/mol, which is lower than that of the Barnett shale (average 62 kcal/mol). When $EasyR_o$ is 0.8%–1.3%, the gas generation potential of Chang 7 shale is 20–80 ml/gTOC, which is higher than that of Barnett shale (18–55 ml/gTOC) (Figure 3). It is an important manifestation of the difference in kerogen properties between lacustrine shale and marine shale in the Yanchang Formation. Taking the TOC of the Yanchang Formation shale as the benchmark of 5%, when it can reach the gas generation potential of 2 m^3/t rock, the organic matter maturity of the kerogen thermal simulation sample is about 1.0% $EasyR_o$ (Figure 4A). The increase of the total organic carbon content can reduce the maturity requirement (Figure 4B).

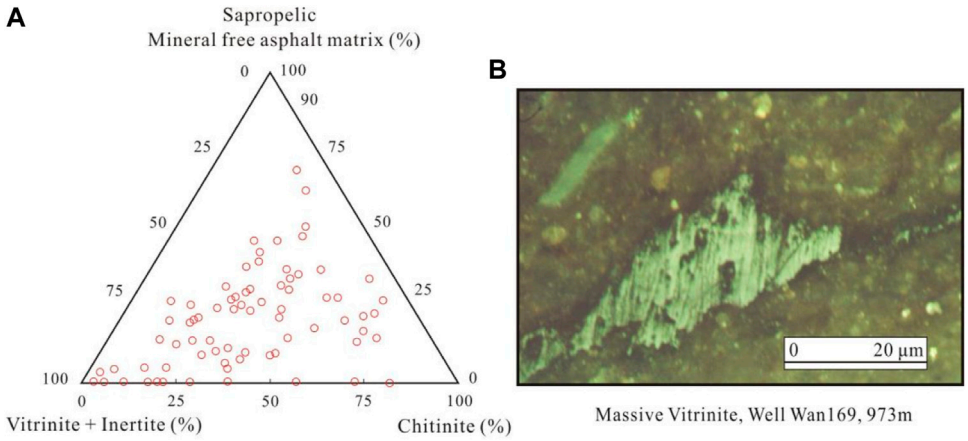

FIGURE 2
Composition of the Chang 7 Member shale in the study area. **(A)** Microscopic composition of kerogen in the Chang 7 member; **(B)** Massive vitrinite structure of the Chang 7 Member shale.

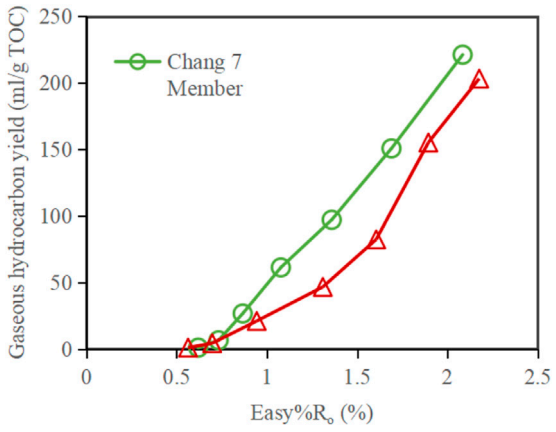

FIGURE 3
Comparison of kerogen gas generation potential between the Yanchang Formation shale and the Barnett Shale.

3.2 Catalysis of pyrite

From the perspective of hydrocarbon generation kinetics, pyrite and aromatic hydrocarbon compounds can also undergo addition reaction under certain conditions to generate organic sulfur-rich kerogen (Kong et al., 2016; Xiong et al., 2017; Mahmoodi et al., 2019; Jiang et al., 2022; Li., 2022). The kerogen rich in organic sulfur can be broken at a relatively low temperature due to the low bond energy of the C-S bond. Pyrite Fe^{2+} is a transition metal, it can significantly affect the electron cloud distribution of cracked organic matter, reduce the activation energy of cracking organic matter, and promote hydrocarbon generation (Loucks et al., 2012; Milliken et al., 2013; Sun et al., 2015; Zhang et al., 2020; Wang et al., 2022). As an inducer, pyrite can promote the formation of hydrocarbons by inducing the formation of free radicals in the process of organic hydrocarbon generation (Wyllie and Spangler, 1952; Tiab and Donaldson., 2004; Roy et al., 2014; Oluwadebi et al., 2019).

The morphological characteristics of pyrite in the Chang 7 Member shale are studied in detail. The analysis shows that a large number of pyrites are developed in the shale of the Chang 7 Member. Vertically, the abundance of pyrite and the content of organic carbon change synergistically, that is, their content has a strong positive correlation. The pyrite content of the Well Yaoye 1 is 0.2%–1% from the bottom of the Chang 7 Member (250–240 m). The pyrite content is very low, even below the detection limit of 5%. At the same depth, the organic carbon content of fine-grained sedimentary rocks does not exceed 5%, generally around 1%. In the 230–220 m interval, the pyrite content gradually increased to more than 10%, and some samples had more than 30% pyrite content. As the pyrite content increased, the organic carbon abundance also increased to above 10%, and some exceeded 25%. In the 220–190 m well section, the pyrite content showed a gradual downward trend, and the content was less than 1%. At the same time, the organic carbon content of the samples was mostly below 3%. Therefore, in the Chang 7 Member shale in the study area, high organic carbon content corresponds to high pyrite content, which is favorable for the formation of shale gas (Figure 5).

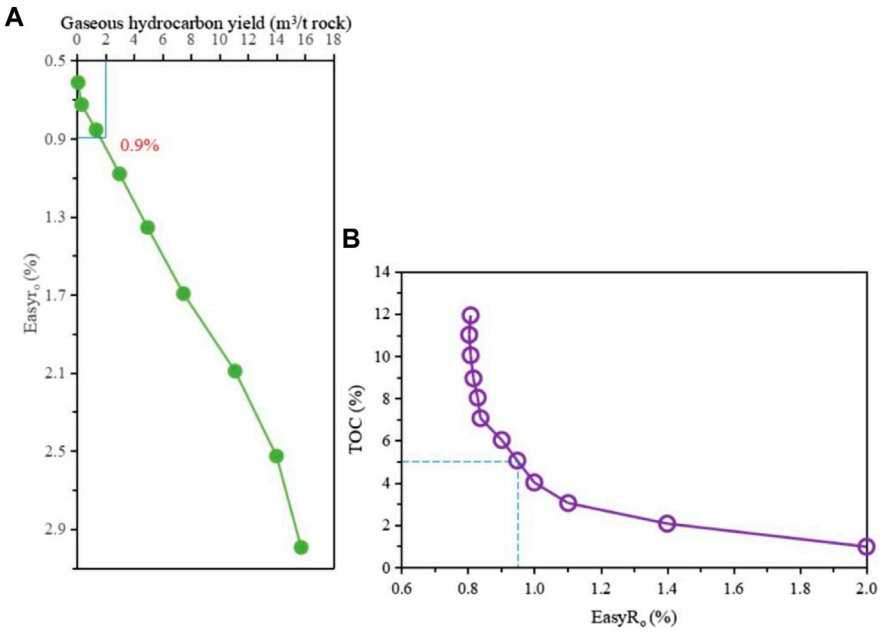

FIGURE 4
Relationship between hydrocarbon generation potential parameters of the Chang 7 Member shale. **(A)** Gas generation potential per unit mass of the Chang 7 shale (based on TOC of 5%); **(B)** Relationship between TOC and EasyRo.

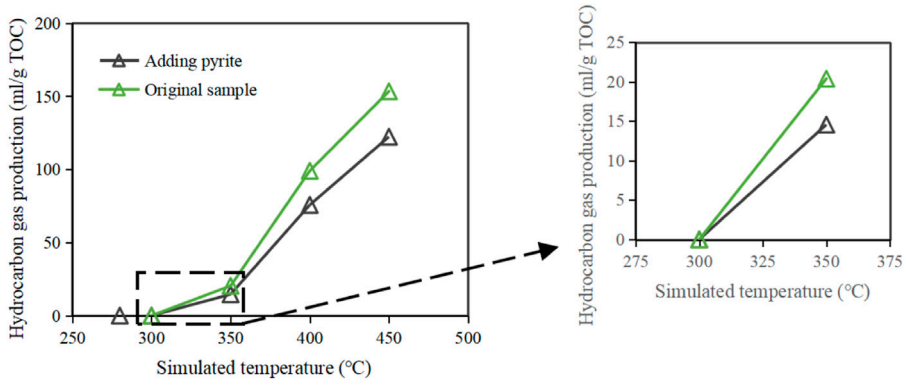

FIGURE 5
Comparison of gas generation potential before and after adding pyrite to the Chang 7 Member shale.

3.3 Characteristics of thermal evolution degree of shale reservoirs

The organic matter of the Chang 7 Member shale is mainly Type II_1, with R_o in the range of 0.5%–1.33%, and has low activation energy of gas generation. These characteristics are favorable for gas generation in mature stage.

During the thermal evolution of kerogen, gases such as methane continue to be generated. For the mixed kerogen of the Yanchang Formation, the generation rate is low in the period of low temperature, which is not conducive to the formation and enrichment of shale gas (Valenza et al., 2013; Wang et al., 2015; Yu Y. et al., 2019). However, stratigraphic uplift that began in the mid-Cretaceous limits the further production of natural gas in the shale. Therefore, in the process of natural gas formation, uplift or temperature decrease caused by tectonic evolution is an important external factor restricting the gas generation process of the Yanchang Formation shale. The analysis of paleo-tectonic

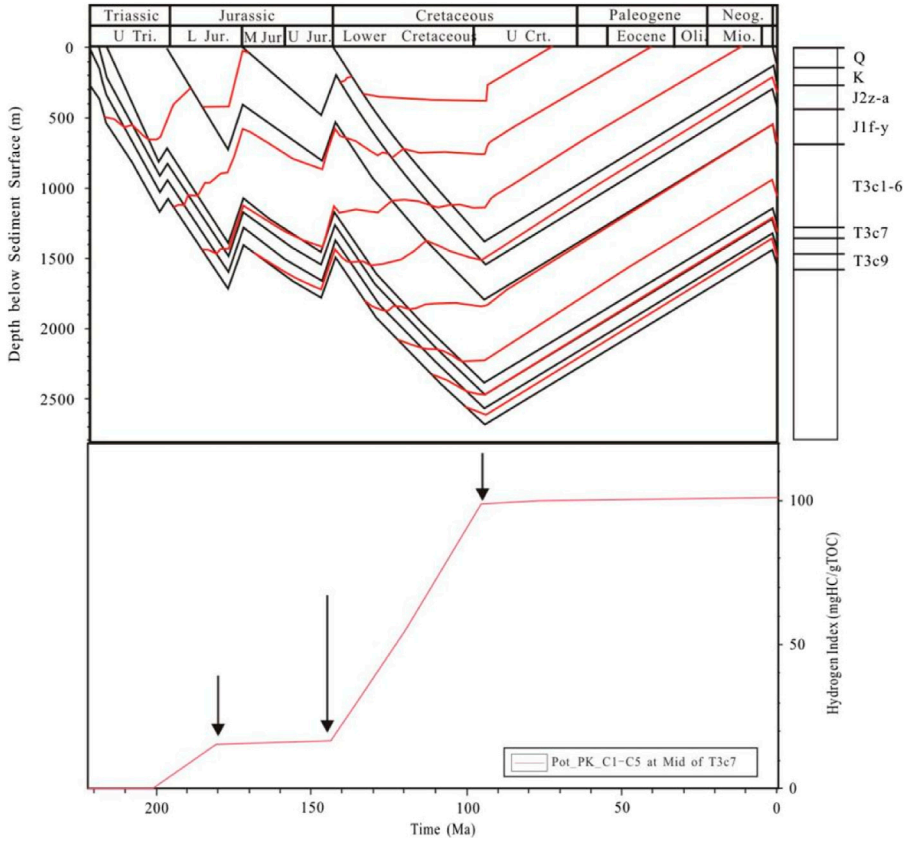

FIGURE 6
Hydrocarbon generation and evolution characteristics revealed by kerogen-enclosed high temperature and high pressure thermal simulation.

restoration and tectonic evolution history shows that the maximum burial depth corresponding to the bottom of the Yanchang Formation in different regions is different, and it is mainly distributed between 2,500 and 3,100 m.

According to the basin simulation results, the evolution process of shale gas generation in the Chang 7 Member in the study area can be divided into four stages (Figure 6): 1) At the end of the Late Triassic (before 200 Ma), there was basically no natural gas generation; 2) From the Early Jurassic to the end of the Late Jurassic (200–145 Ma), the generation rate of natural gas was low, and the generation of natural gas was stagnant due to structural uplift; 3) From the Late Jurassic to the end of the Early Cretaceous (145–95 Ma), the Yanchang Formation was rapidly buried and matured, and it was a period of massive natural gas generation; 4) From the end of the Early Cretaceous to the present (95 Ma-), the strata were uplifted and denuded, the gas generation rate of shale was greatly reduced, and the gas generation stopped. Under geological conditions, the cumulative gas conversion rate of the Yanchang Formation shale is about 30%.

The Trinity Basin Simulation System was used to evaluate the gas generation potential. According to the shale thickness and total organic carbon (TOC) content of the target layer, the gas generation intensity and potential of shale in different layers are calculated. The evaluation results show that the current cumulative maximum gas generation intensity of the Chang 7 Member shale in the study area is 9×10^8 m^3/km^2. The center of gas intensity is located in the areas of the Danba, Xiasiwan and Zhangjiawan cities. Field analysis shows that the total gas content of the Chang 7 Member shale ranges from 2.10 to 5.23 m^3/t, with an average of 3.8 m^3/t; the adsorbed gas content is 65%–85%, with an average of 70%; and the average free gas content is 20%. In addition to alkane gas, the gas components in the target layer also include non-hydrocarbon gases such as carbon dioxide and nitrogen. The content of heavy hydrocarbons in the hydrocarbon gas component is high, and the drying coefficient of the gas is generally low, and the drying coefficient (C_1/C_{1-5}) is generally lower than 0.95. This shows that the shale gas in this area is mainly wet gas (Figure 7).

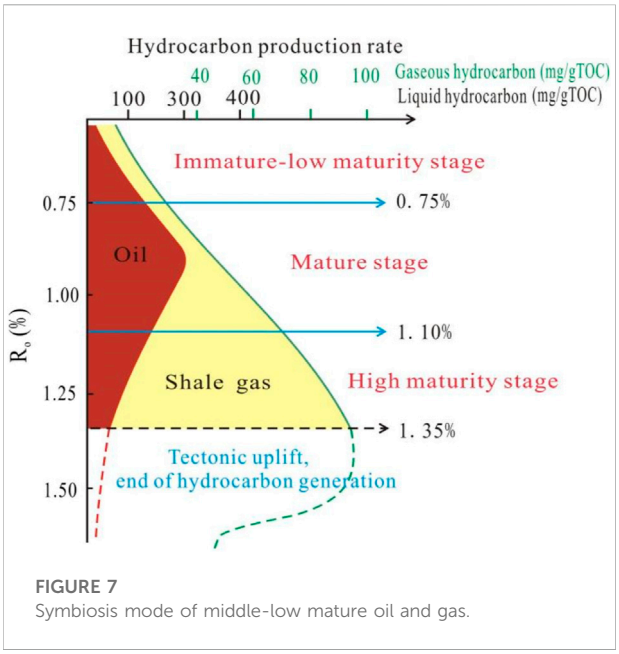

FIGURE 7
Symbiosis mode of middle-low mature oil and gas.

4 Discussion

4.1 Analysis of shale gas occurrence conditions based on multi-type and cross-scale complex pore network

Spaces of porous reservoir of various types and scales are the places where oil and gas occur in shale. The observation results under the microscope show that the residual intergranular pores between rigid clastic grains and intercrystalline pores of clay minerals are developed in the shale. Part of the edges of the intergranular pores were eroded to form erosion enlarged pores. The pore size of the intergranular pores in the Yanchang Formation shale is mainly ranges from 5 to 600 nm, with a maximum of 3.4 μm, and the pore size of most pores is less than 200 nm, with an average of 75 nm (Figure 8). Intragranular pores include intragranular dissolved pores such as feldspar and calcite, mold pores, intragranular pores in aggregates such as clay mineral aggregates and strawberry-like pyrite, and fossil cavity pores. The pore size of the intragranular pores in the Yanchang Formation shale is mostly less than 200 nm, and the maximum value can reach 4.7 μm. The intragranular pores with larger pore sizes are dissolved pores of feldspar particles, and the peak pore size is 20–30 nm.

The macropores of the Yanchang Formation shale are mainly occupied by free gas, followed by liquid hydrocarbons, and the volume of adsorbed gas is negligible.

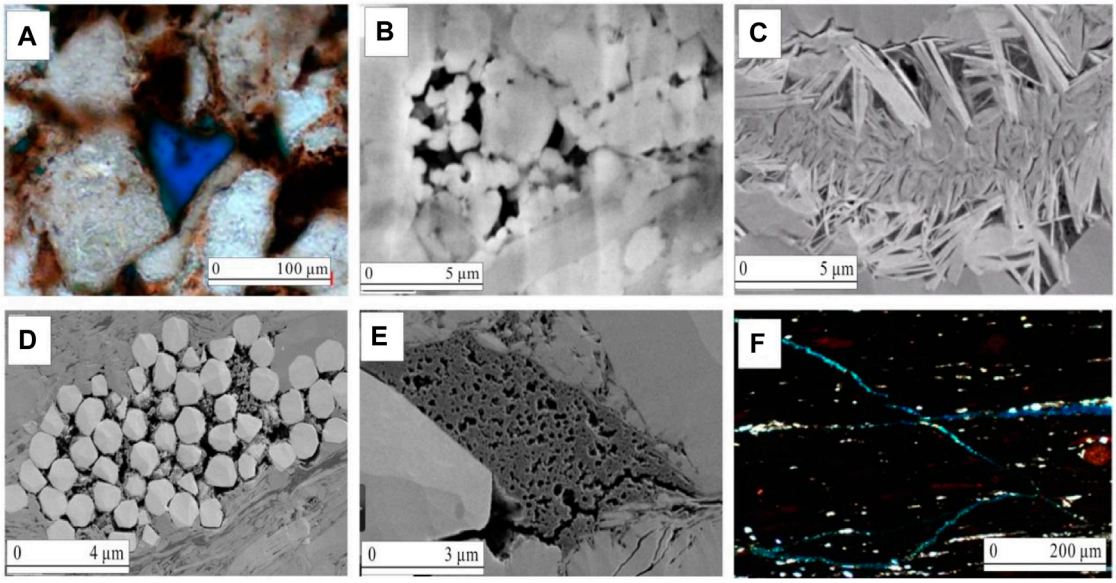

FIGURE 8
Micrographs of pore types in the Chang 7 shale. **(A)** Residual intergranular pores in siltstone interlayer, Well YY3, single polarized light, 1,325 m; **(B)** Intergranular dissolution pores, SEM, Well YY8, 1,522.8 m; **(C)** Intragranular pores of clay mineral aggregates, SEM, Well YY7, 1,140.1 m; **(D)** Intragranular pores of pyrite aggregates, SEM, Well YY22, 1,299.73 m; **(E)** Organic pores filled with organic matter in the inorganic intergranular pores between the debris particles, SEM, Well YY6, 1,307.32 m; **(F)** Laminates and bedding fractures, cross polarized light, Well YY11, 1,378.37 m).

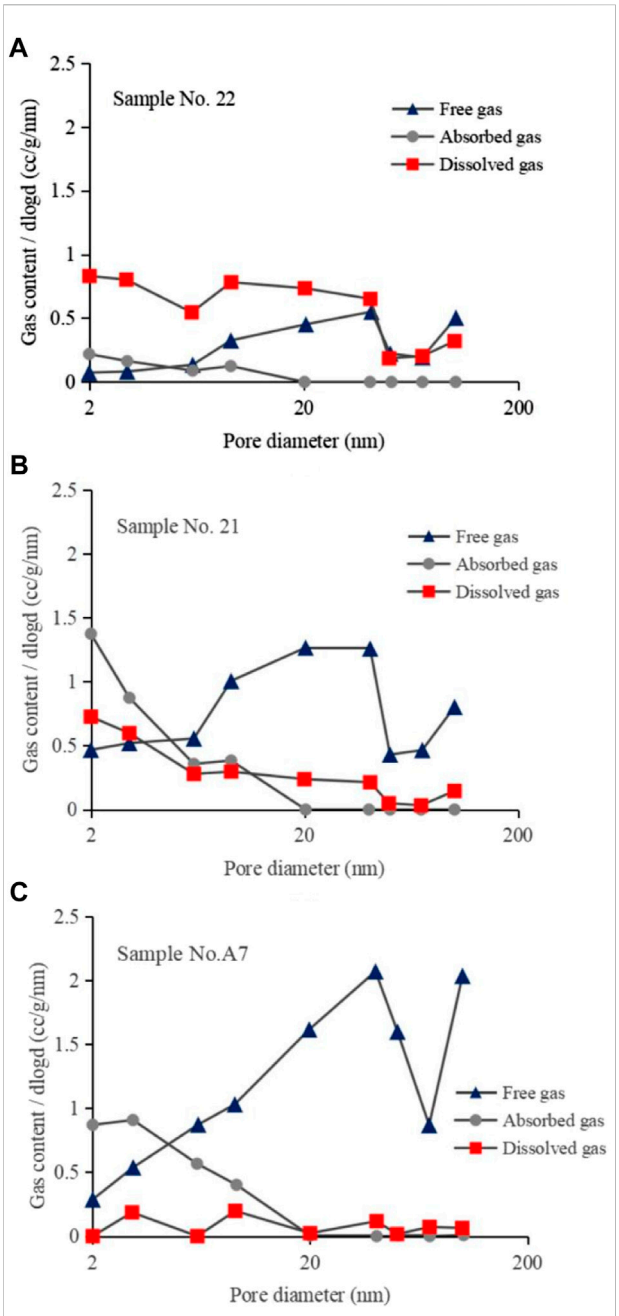

FIGURE 9
Occurrence volumes of various phase fluids in different pores in the 2–100 nm pore size range (25°C, 13 MPa). **(A)** Sample No. 22; **(B)** Sample No. 21; **(C)** Sample No. A7.

The ratio of adsorbed gas to free gas is 3:7. On the whole, the volume proportion of liquid hydrocarbons in the macropores of the three rock types is generally low (below 30%), with an average of 15%. Some siltstones (No. 34) and silt-bearing laminar shale (No. 21) have a relatively high volume of liquid hydrocarbons in large pores, accounting for 45% and 31%, respectively (Figure 9).

Figure 9 shows the volume changes of adsorbed gas, free gas and liquid hydrocarbons in the meso-macropores from 2 to 100 nm. The volume occupied by free gas in the pores generally increases with the increase of the pore size. In the silty laminar shale (A4, A7) and siltstone with low liquid hydrocarbon content, the pore volume occupied by free gas is always higher than that of liquid hydrocarbons (Wang et al., 2020; Yoshida and Santosh., 2020; Xu et al., 2022). Moreover, in the range of pore size >10 nm, the free gas storage volume in the pores increases rapidly. In argillaceous shale and silt-bearing laminar shale (No. 22 and 31) with high liquid hydrocarbon content, the pore volume occupied by liquid hydrocarbons is larger than that occupied by free gas in the pore size range of 2–10 nm. With the increase of pore size, the overall volume of free gas in the pores increases slowly, and the pore volume occupied by free gas and liquid hydrocarbons is basically the same.

On the whole, as the pore size increases, the free gas saturation in the pores increases rapidly, the adsorbed gas saturation decreases rapidly, and the overall variation of the dissolved gas saturation is relatively low (Yan et al., 2015; Zhang et al., 2019). Among them, some siltstones (No. 34) and silt-bearing laminar shale (No. A4) have high liquid hydrocarbon content in large pores with a diameter of more than 100 nm.

4.2 Control of diagenetic stage and thermal evolution on shale pore evolution

Combined with the results of this paper, a mode of shale pore evolution in the Yanchang Formation shale in the study area was proposed (Figure 10). The mode is divided into the following four stages: 1) Early diagenetic stage (R_o < 0.5%). At this stage, the hydrocarbon generation of organic matter is not obvious, and the diagenesis is dominated by mechanical compaction. Compaction affects the rapid reduction of pores; 2) Middle diagenetic stage A (0.5% < R_o< 1.2%). In this stage, the hydrocarbon generation of organic matter will produce organic acids to dissolve minerals such as feldspar, and on the other hand, there will be hydrocarbon generation pressurization. The diagenesis at this stage is dominated by the transformation of clay minerals. In addition, because the rock is in the oil-generating window as a whole, the compaction has a great influence, and the combination of these effects causes the pores to first decrease, then increase, and then decrease. 3) Middle diagenetic stage B (1.2% < R_o< 2%). At this stage, due to the organic matter entering the gas window, the hydrocarbon generation of organic matter leads to the development of a large number of organic pores. However, the dissolution effect of organic acid and hydrocarbon generation pressurization are not obvious at this stage. In addition, the transformation of clay minerals in diagenesis

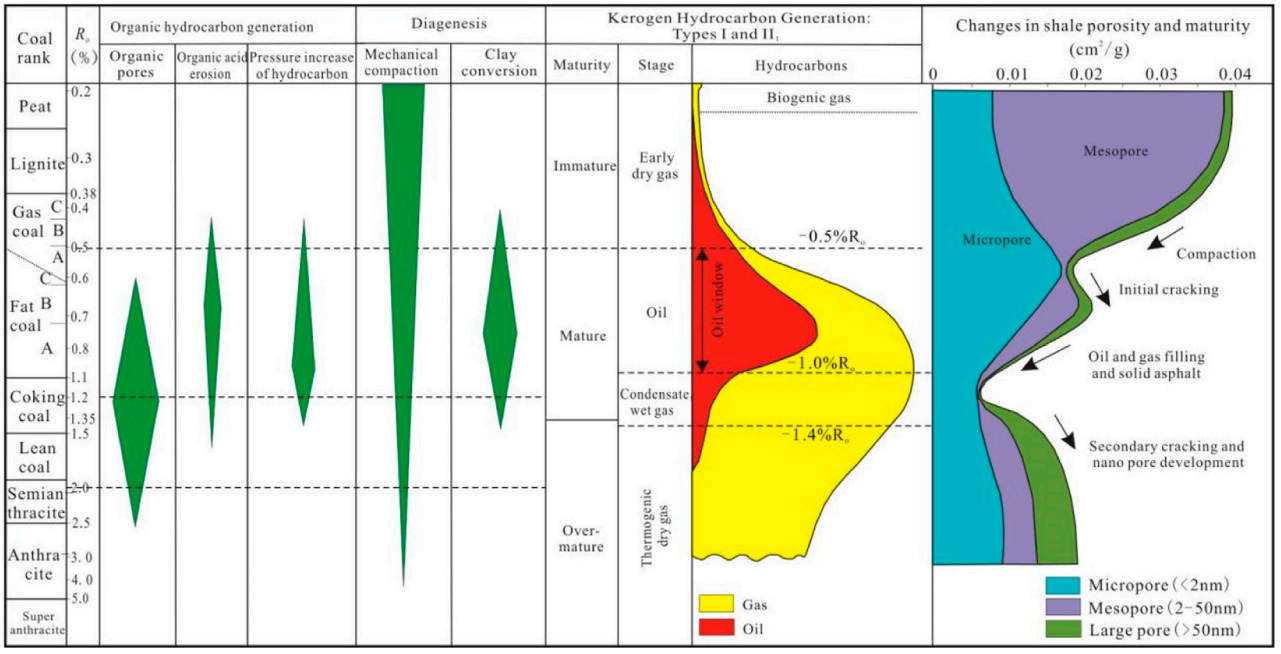

FIGURE 10
Evolution mode of pores in the Chang 7 Member shale in Yan'an area.

also basically stopped. As the compressive strength of rock increases, the effect of compaction on pores is further reduced. The combination of these effects leads to a continuous increase in porosity; 4) Late diagenetic stage (R_o > 2.0%). The effect of organic hydrocarbon generation is very weak, and the effect of compaction on pores is also very small. The pores are in a relatively stable state with small changes.

4.3 Self-sealing ability of thick shale and control of high pressure on shale gas preservation

4.3.1 Hydrocarbon expulsion limit

In the Ordos Basin, the tectonic activity in the Yanchang Formation is weak, the structure is relatively flat, and the open faults are not developed. The overlying thick mudstones, rather than structure, is the controlling factor for the preservation conditions of lacustrine shale gas. According to the distribution characteristics of parameters in laboratory experiments, gas logging and logging interpretation, there are differences in hydrocarbon expulsion in shale layers. The shale interval adjacent to the sandstone preferentially expels hydrocarbons and has a lower residual hydrocarbon content. Moreover, there is a thickness limit in the hydrocarbon expulsion section, and the effective hydrocarbon expulsion thickness is 8–12 m. The thickness of the lacustrine shale in the Chang 7 Member is relatively large (40–120 m), which exceeds the thickness limit of effective hydrocarbon expulsion in this area. Therefore, it has the characteristics of "self-sealing by thick mudstone cap".

4.3.2 Excess pressure

Excess pressure is the difference between actual pressure and hydrostatic pressure. The excess pressure at the maximum burial depth of shale is the main driving force for source rocks to expel hydrocarbons. The simulation calculation and actual measurement results show that the excess pressure of the Chang 7 Member at the end of the Early Cretaceous was between 5 and 30 MPa. And its overall distribution is a nearly north-south strip-like distribution, and the excess pressure value is between 10 and 20 MPa (Figure 11). The study found that the higher the abnormal high pressure value generated in the strata at the end of the Early Cretaceous, the richer the shale gas. This is because the larger the abnormal high pressure value generated in the formation, the better the sealing performance and the better the preservation conditions are. At the end of the Early Cretaceous, the excess pressure of the Chang 7 Member shale was basically above 3 MPa. The larger pressure difference has a good sealing ability for the shale gas in the laminae, so that the gas can be preserved for a long time.

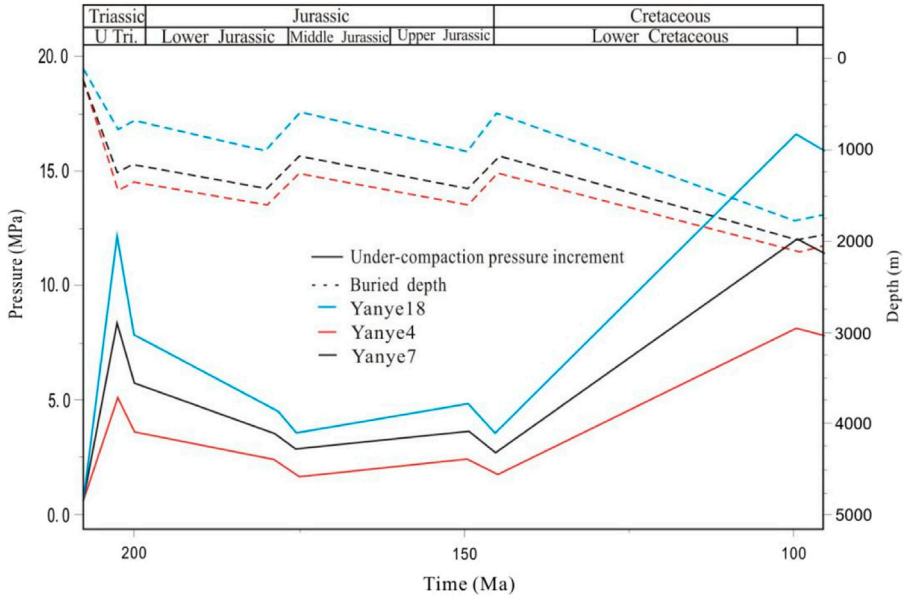

FIGURE 11
Evolution of excess pressure during disequilibrium compaction in the Chang 7 Member shale.

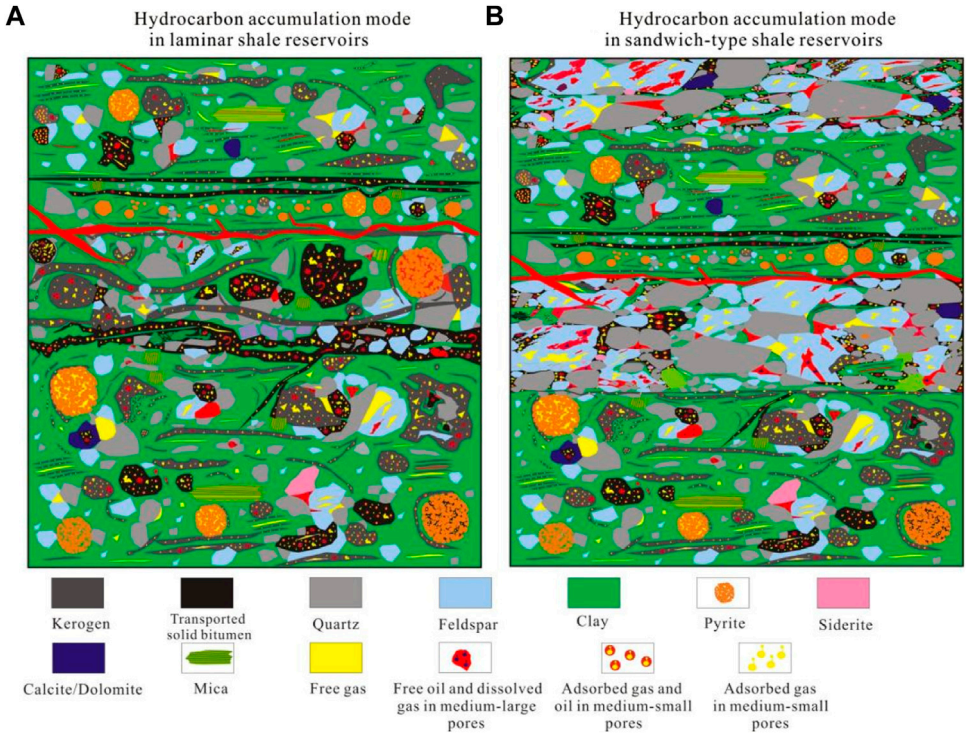

FIGURE 12
Accumulation patterns of hydrocarbons in lacustrine shale. **(A)** Hydrocarbon accumulation pattern of laminar shale gas reservoirs; **(B)** Hydrocarbon accumulation pattern in sandwich-type shale gas reservoirs.

4.4 Hydrocarbon accumulation modes and sweet spot types

As a "layered gas reservoir" with continuous distribution, the large-scale accumulation of shale gas requires basic geological conditions. Simply put, the gas source layer determines how much shale gas is produced, the reservoir determines where the shale gas exists, and the preservation conditions determine how much shale gas is left. The unity of "gas source layer, reservoir and cap layer" together constitutes the "ternary" controlling factors of shale gas enrichment. The accumulation modes of shale gas include the laminar type (with thick shale laminae) mode (Figure 12A) and the sandwich type (shale with thin sandstone) mode (Figure 12B).

4.4.1 Laminar type (with thick shale laminae) mode

This type of mode is mainly distributed in the lower part of the Chang 7 Member, that is, the gas accumulation mode of thick shale with sandy laminae. The organic carbon content of shale is more than 2%, R_o is 0.7%–1.1%, and a certain amount of crude oil associated gas is generated. The internal storage space of shale is mainly composed of intergranular pores, intercrystalline pores and a small amount of organic pores, and the porosity is 2%–6%. The driving force of hydrocarbon gas expulsion is mainly source-reservoir pressure difference (5–10 MPa), and hydrocarbons experience small-scale migration. The preservation condition is the formation pressure formed at the maximum burial depth at the end of the Early Cretaceous, and it is the residual pressure today. At the same time, the thick mudstone interlaced with the laminae also has a controlling effect on the preservation of shale gas.

4.4.2 Sandwich type (shale with thin sandstone) mode

The TOC of this type of shale is 1%–2%, the R_o is greater than 2.0%, and a large amount of hydrocarbon gas is generated, which is basically dry gas. The reservoir space is mainly intergranular pores, intercrystalline pores and intergranular dissolution pores, and the porosity is 2%–8%. Moreover, the driving force of hydrocarbon expulsion is mainly the pressure difference between source and reservoir, which is 3–5 MPa. At the same time, the thick mudstone intertwined with the sandstone has a controlling effect on the preservation of shale gas.

5 Conclusion

1) The Chang 7 Member in the Yanchang Formation has the basic gas generating conditions for shale gas. Shale gas accumulation in the Chang 7 Member requires three necessary accumulation elements, namely gas source, reservoir and good preservation conditions. The dynamic hydrocarbon generation process of shale reservoirs is established according to the thermal simulation experiment of hydrocarbon generation, and the mechanism of catalytic degradation and gas generation in the Chang 7 Member under the background of low thermal evolution is revealed.
2) The enriched authigenic pyrite can catalyze the hydrocarbon generation of organic matter with low activation energy, thereby increasing the hydrocarbon generation rate in the low-mature-mature stage. Different types of pores at different scales (2–100 nm) form a multi-scale complex pore network. Free gas and dissolved gas are enriched in laminar micro-scale pores, and adsorbed gas is enriched in nano-scale pores of thick shale, and silty laminates can improve the physical properties of the reservoir. This is because the laminar structure has better hydrocarbon generation conditions and is favorable for the migration of oil and gas molecules.
3) The thickness of lacustrine shale in the Chang 7 Member is between 40 and 120 m, which exceeds the effective hydrocarbon expulsion thickness limit (8–12 m) in the study area. At the end of the Early Cretaceous, the excess pressure of the Chang 7 shale was above 3 MPa. At present, horizontal wells with a daily gas production of more than 50,000 cubic meters are distributed in areas with high excess pressure during the maximum burial depth.

Data availability statement

The original contributions presented in the study are included in the article/supplementary material, further inquiries can be directed to the corresponding author.

Author contributions

XW and CG are responsible for the idea and writing of this paper and QL, PX, JY, and SH are responsible for the experiments and analysis.

Funding

This research was supported by the Major national science and technology project "Key technologies for exploration and development of lacustrine shale gas in Yan'an area (No. 2017zx05039)", the Key R&D Plan of Shaanxi Province, "Research on efficient CO_2 replacement mechanism and technology for Lacustrine high adsorption shale gas in Yanchang Exploration area (No. 2022GY-138)", and the Research Project of Yanchang Oil Field Co., Ltd., "Dynamics genesis mechanism and differential evolution of fine grain sedimentary in Lacustrine shale oil and gas reservoirs of Yanchang Formation in Yanchang Exploration area (ycsy2022jcts-B-49)".

Conflict of interest

Authors XW, QL, CG, PX, JY and SH were employed by the company Shaanxi Yanchang Petroleum (Group) Corp., Ltd.

Publisher's note

References

Asante-Okyere, S., Ziggah, Y. Y., and Marfo, S. A. (2021). Improved total organic carbon convolutional neural network model based on mineralogy and geophysical well log data. *Unconv. Resour.* 1, 1–8. doi:10.1016/j.uncres.2021.04.001

Fan, C. H., Li, H., Qin, Q. R., Shang, L., Yuan, Y. F., and Li, Z. (2020). Formation mechanisms and distribution of weathered volcanic reservoirs: A case study of the carboniferous volcanic rocks in Northwest Junggar Basin, China. *Energy Sci. Eng.* 8 (8), 2841–2858. doi:10.1002/ese3.702

Hong, D., Cao, J., Wu, T., Dang, S., Hu, W., and Yao, S. (2020). Authigenic clay minerals and calcite dissolution influence reservoir quality in tight sandstones: Insights from the central Junggar Basin, NW China. *Energy Geosci.* 1 (1–2), 8–19. doi:10.1016/j.engeos.2020.03.001

Ji, L., Zhang, T., Milliken, K. L., Qu, J., and Zhang, X. (2012). Experimental investigation of main controls to methane adsorption in clay-rich rocks. *Appl. Geochem.* 27, 2533–2545. doi:10.1016/j.apgeochem.2012.08.027

Jiang, W., Zhang, P., Li, D., Li, Z., Wang, J., Duan, Y., et al. (2022). Reservoir characteristics and gas production potential of deep coalbed methane: Insights from the no. 15 coal seam in Shouyang block, Qinshui Basin, China. *Unconv. Resour.* 2, 12–20. doi:10.1016/j.uncres.2022.06.001

Katz, B., Gao, L., Little, J., and Zhao, Y. R. (2021). Geology still matters – Unconventional petroleum system disappointments and failures. *Unconv. Resour.* 1, 18–38. doi:10.1016/j.uncres.2021.12.001

Kong, L., Wan, M., Yan, Y., Zou, C., Liu, W., Tian, C., et al. (2016). Reservoir diagenesis research of silurian longmaxi Formation in Sichuan Basin, China. *J. Nat. Gas Geoscience* 23, 203–211. doi:10.1016/j.jnggs.2016.08.001

Lama, R., and Vutukuri, V. (1978). *Handbook on mechanical properties of rocks, vol II*. Clausthal, Germany: Trans Tech Publications, 58–60. doi:10.1016/0013-7952(75)90018-6

Lan, S. R., Song, D. Z., Li, Z. L., and Liu, Y. (2021). Experimental study on acoustic emission characteristics of fault slip process based on damage factor. *J. Min. Strata Control Eng.* 3 (3), 033024. doi:10.13532/j.jmsce.cn10-1638/td.20210510.002

Li, G., Qin, Y., Wu, M., Zhang, B., Wu, X., Tong, G., et al. (2019). The pore structure of the transitional shale in the Taiyuan formation, Linxing area, Ordos Basin. *J. Petroleum Sci. Eng.* 181, 106183–106186. doi:10.1016/j.petrol.2019.106183

Li, H. (2022). Research progress on evaluation methods and factors influencing shale brittleness: A review. *Energy Rep.* 8, 4344–4358. doi:10.1016/j.egyr.2022.03.120

Liang, L., Xiong, J., Liu, X., and Luo, D. (2016). An investigation into the thermodynamic characteristics of methane adsorption on different clay minerals. *J. Nat. Gas Sci. Eng.* 33, 1046–1055. doi:10.1016/j.jngse.2016.06.024

Loucks, R. G., Reed, R. M., Ruppel, S. C., and Hammes, U. (2012). Spectrum of pore types and networks in mudrocks and a descriptive classification for matrix-related mudrock pores. *Am. Assoc. Pet. Geol. Bull.* 96, 1071–1098. doi:10.1306/08171111061

Mahmoodi, S., Abbasi, M., and Sharifi, M. (2019). New fluid flow model for hydraulic fractured wells with non-uniform fracture geometry and permeability. *J. Nat. Gas Sci. Eng.* 68, 102914–14. doi:10.1016/j.jngse.2019.102914

Mahmud, H., Hisham, M., Mahmud, M., Leong, V., and Shafiq, M. (2020). Petrophysical interpretations of subsurface stratigraphic correlations, Baram Delta, Sarawak, Malaysia. *Energy Geosci.* 1 (3–4), 100–114. doi:10.1016/j.engeos.2020.04.005

Milliken, K. L., Rudnicki, M., Awwiller, D. N., and Zhang, T. (2013). Organic matter-hosted pore system, Marcellus Formation (Devonian), Pennsylvania. *Am. Assoc. Pet. Geol. Bull.* 97, 177–200. doi:10.1306/07231212048

Oluwadebi, A., Taylor, K., and Ma, L. (2019). A case study on 3D characterisation of pore structure in a tight sandstone gas reservoir: The Collyhurst Sandstone, East Irish Sea Basin, Northern England. *J. Nat. Gas Sci. Eng.* 68, 102917–17. doi:10.1016/j.jngse.2019.102917

Qie, L., Shi, Y. N., and Liu, J. S. (2021). Experimental study on grouting diffusion of gangue solid filling bulk materials. *J. Min. Strata Control Eng.* 3 (2), 023011. doi:10.13532/j.jmsce.cn10-1638/td.20201111.001

Roy, B., Hart, B., Mironnova, A., Zhou, C. X., and Zimmer, U. (2014). Integrated characterization of hydraulic fracture treatments in the Barnett shale: The Stocker geophysical experiment. *Interpretation* 2 (2), T111–T127. doi:10.1190/INT-2013-0071.1

Santosh, M., and Feng, Z. Q. (2020). New horizons in energy geoscience. *Energy Geosci.* 1 (1–2), 1–3. doi:10.1016/j.engeos.2020.05.005

Sun, M., Yu, B., Hu, Q.-H., Chen, S., Xia, W., and Ye, R. (2015). Nanoscale pore characteristics of the Lower Cambrian Niutitang Formation Shale: A case study from Well Yuke #1 in the Southeast of Chongqing, China. *Int. J. Coal Geol.* 154, 16–29. doi:10.1016/j.coal.2015.11.015

Sun, Z., Wang, Y., Wei, Z., Zhang, M., Wang, D., Wang, Z., et al. (2017). Shale gas content and geochemical characteristics of marine-continental transitional shale: A case from the Shanxi formation of Ordos Basin. *J. China Univ. Min. Technol.* 46 (4), 859–868.

Tiab, D., and Donaldson, E. C. (2004). *Petrophysics: Theory and practice of measuring reservoir rock and fluid transport properties*. Elsevier, 56–59.

Ursula, I. V., and Jorge, O. P. (2014). Artificial neural networks applied to estimate permeability, porosity and intrinsic attenuation using seismic attributes and well- log data. *J. Appl. Geophys.* 107, 45–54. doi:10.1016/j.jappgeo.2014.05.010

Vafaie, A., Kivi, I. R., Moallemi, S. A., and Habibnia, B. (2021). Permeability prediction in tight gas reservoirs based on pore structure characteristics: A case study from South Western Iran. *Unconv. Resour.* 1, 9–17. doi:10.1016/j.uncres.2021.08.001

Valenza, J. J., Drenzek, N., Marques, F., Pagels, M., and Mastalerz, M. (2013). Geochemical controls on shale microstructure. *Geology* 41 (5), 611–614. doi:10.1130/G33639.1

Wang, G., Ju, Y., Yan, Z., and Li, Q. (2015). Pore structure characteristics of coal–bearing shale using fluid invasion methods: A case study in the huainan–huaibei coalfield in China. *Mar. Petroleum Geol.* 62, 1–13. doi:10.1016/j.marpetgeo.2015.01.001

Wang, H., Shi, Z., Zhao, Q., Liu, D., Sun, S., Guo, W., et al. (2020). Stratigraphic framework of the Wufeng-Longmaxi shale in and around the Sichuan Basin, China: Implications for targeting shale gas. *Energy Geosci.* 1 (3–4), 124–133. doi:10.1016/j.engeos.2020.05.006

Wang, H., Zhou, S., Li, S., Zhao, M., and Zhu, T. (2022). Comprehensive characterization and evaluation of deep shales from Wufeng-Longmaxi Formation by LF-NMR technology. *Unconv. Resour.* 2, 1–11. doi:10.1016/j.uncres.2022.05.001

Wu, J. S., and Yu, B. M. (2007). A fractal resistance model for flow through porous media. *Int. J. Heat Mass Transf.* 50 (19), 3925–3932. doi:10.1016/j.ijheatmasstransfer.2007.02.009

Wyllie, M. R. J., and Spangler, M. B. (1952). Application of electrical resistivity measurements to problem of fluid flow in porous media. *AAPG Bull.* 36, 359–403. doi:10.3406/geo.1951.13171

Xiong, F., Jiang, Z., Li, P., Wang, X., Bi, H., Li, Y., et al. (2017). Pore structure of transitional shales in the Ordos Basin, NW China: Effects of composition on gas storage capacity. *Fuel* 206, 291062–291515. doi:10.1130/abs/2017NE-291062

Xu, H., Zhou, W., Hu, Q., Xia, X., Zhang, C., and Zhang, H. (2019). Fluid distribution and gas adsorption behaviors in over-mature shales in southern China. *Mar. Petrol. Geol.* 109, 223–232. doi:10.1016/j.marpetgeo.2019.05.038

Xu, Z., Cheng, Y., Ao, C., Zhang, T., and Wang, S. (2022). Middle Jurassic palaeoclimate changes within the central Ordos Basin based on palynological records. *Paleobiodivers. Paleoenviron.* 13, 1–13. doi:10.1007/s12549-021-00518-8

Xue, F., Liu, X. X., and Wang, T. Z. (2021). Research on anchoring effect of jointed rock mass based on 3D printing and digital speckle technology. *J. Min. Strata Control Eng.* 3 (2), 023013. doi:10.13532/j.jmsce.cn10-1638/td.20201020.001

Yan, D., Huang, W., and Zhang, J. (2015). Characteristics of marine continental transitional organic rich shale in the Ordos Basin and its shale gas significance. *Earth Sci. Frontiers* 22 (6), 197–206. doi:10.13745/j.esf.2015.06.015

Yang, C., Zhang, J., Tang, X., Ding, J., Zhao, Q., Dang, W., et al. (2016). Comparative study on micro-pore structure of marine, terrestrial, and transitional shales in key areas, China. *Int. J. Coal Geol.* 171, 76–92. doi:10.1016/j.coal.2016.12.001

Yoshida, M., and Santosh, M. (2020). Energetics of the Solid Earth: An integrated perspective. *Energy Geosci.* 1 (1–2), 28–35. doi:10.1016/j.engeos.2020.04.001

Yu, K., Shao, C., Ju, Y., and Qu, Z. (2019a). The Genesis and controlling factors of micropore volume in transitional coal-bearing shale reservoirs under different sedimentary environments. *Mar. Petroleum Geol.* 102, 426–438. doi:10.1016/j.marpetgeo.2019.01.003

Yu, Y., Luo, X., Wang, Z., Cheng, M., Lei, Y., Zhang, L., et al. (2019b). A new correction method for mercury injection capillary pressure (MICP) to characterize the pore structure of shale. *J. Nat. Gas Sci. Eng.* 68, 102896–102905. doi:10.1016/j.jngse.2019.05.009

Zhang, D., Li, S., and Zhang, X. (2020). Experimental study on mining fault activation characteristics by a distributed optical fiber system. *J. Min. Strata Control Eng.* 2 (1), 013018. doi:10.13532/j.jmsce.cn10-1638/td.2020.01.010

Zhang, M., Fu, X., Zhang, Q., and Cheng, W. J. J. (2019). Research on the organic geochemical and mineral composition properties and its influence on pore structure of coal-measure shales in Yushe-Wuxiang Block, South Central Qinshui Basin, China. *J. Petrol. Sci. Eng.* 34, 1065–1079. doi:10.1016/j.petrol.2018.10.079

Zhao, W., Li, J., Yang, T., Wang, S., and Huang, J. (2016). Geological difference and its significance of marine shale gases in South China. *Petroleum Explor. Dev.* 43, 547–559. doi:10.1016/S1876-3804(16)30065-9

Zheng, H., Zhang, J., and Qi, Y. (2020). Geology and geomechanics of hydraulic fracturing in the Marcellus shale gas play and their potential applications to the Fuling shale gas development. *Energy Geosci.* 1 (1–2), 36–46. doi:10.1016/j.engeos.2020.05.002